VNU Journal of Science: Mathematics – Physics, Vol. 38, No. 2 (2022) 71-81

VNU Journal of Science: Mathematics - Physics

Journal homepage: https://js.vnu.edu.vn/MaP

Original Article

Electric Field as A Novel Switch to Enhance Optical Absorption Spectra of Defect Blue Phosphorene Thin-films

Nguyen Vo Anh Duy[1], Dang Minh Triet[2,*], Dinh Van An[3]

[1]*FPT University, Can Tho Campus, 600 Nguyen Van Cu Road, Can Tho City, Vietnam*

[2]*School of Education, Can Tho University, 3-2 Road, Can Tho City, Vietnam*

[3]*Department of Precision Engineering, Graduate School of Engineering, Osaka University, 2-1 Yamadaoka, Suita, Osaka 565-0871, Japan*

Received 23 October 2021
Revised 24 February 2022; Accepted 19 March 2022

Abstract: Improvement of the optical absorption coefficient is essential to enhance the light conversion efficiency of thin-film organic solar cells. Here we report the use of an external electric field as a novel switch to improve the optical absorption capacity of two-dimensional defect blue phosphorene (BlueP) systems. Using the density functional theory with van der Waals functionals, we investigate the structural, electronic, magnetic and optical absorption properties of the pristine, single-vacancy (SV) BlueP thin films, and a BlueP system absorbing a Vanadium adatom. We demonstrate that a SV BlueP layer would exhibit half-metallic and its absorption spectrum under an electric field parallel to the material plane is significantly enhanced in the ultra-violet region. More interestingly, when a Vanadium transition metal is absorbed on a pristine BlueP, the applied electric field perpendicular to the BlueP plane not only doubles the optical absorption coefficient, but also switches ON/OFF the magnetic moments of this system. The prominent red shift of the absorption spectra towards the visible light range under selected polarized directions paves a novel way to engineer solar cell devices with BlueP materials.

Keywords: Optical properties, magnetic properties, two-dimensional blue phosphorene, solar cells.

1. Introduction

Recently, two-dimensional (2D) materials such as silicene [1], borophene [2], phosphorene [3, 4], GaN [5], and transition metal dichalcogenides (TMDs) [6] with unique electronic, optical, and spintronic properties have received enormous attention in the semiconductor industry. Among this class of

* Corresponding author.
E-mail address: dmtriet@ctu.edu.vn

https//doi.org/10.25073/2588-1124/vnumap.4683

materials, phosphorene and its related morphological configurations with indirect bandgaps in the range of 0.90 and 1.53 eV as well as highly mobile charge carriers [3, 7] have been theoretically predicted as a potential candidate for applications in photovoltaic solar devices. Recent breakthrough of molecular beam epitaxy (e.g. [3, 4, 8]) demonstrates the possibility to grow large areas of high-quality monolayer blue phosphorene (BlueP). This potential application for solar panels opens a new route to assemble photovoltaic devices with higher efficiencies. However, in these early new proposed experiments, the direct relation between the opto-electronic properties and the assembled structures is still missing.

Material defect is an avoidable problem during fabrication. The presence of defect sites may significantly alter the electronic, magnetic and optical responses of 2D systems. Phosphorene was predicted to become a dilute magnetic semiconductor when absorbing transition metals or with a certain numbers of Phosphorous (P) atom removal [9, 10]. Thus, it is useful to introduce defect sites to 2D materials to tune their magnetic and electronic properties. However, in terms of versatility and convenience, controlling the opto-electronic properties of 2D materials via structural modification is experimentally difficult, especially in controlling the number of defect sites in the thin films. Consequently, in this study, we propose a more versatile and usable for applications via an external electric field as a novel switch to control the electronic, magnetic, and optic properties of pristine and defective BlueP. This technique is particularly promising since precise electric field control of 2D materials is well-established in semiconductor industry. Using first-principles calculations, through the analyses of the electronic structure using density of states (DOS) and by adding an additional charge carrier to the systems, we provide insightful understanding how the magnetic moment and the optical responses of the defective systems change with the applied electric field. These findings shed light into the use of external electric fields in controlling the opto-electronic properties of BlueP thin-films and open the door to engineer BlueP materials with precisely dedicated optical and electronic properties for solar cell devices.

2. Theoretical Background

We carried out first-principles calculation within density functional theory (DFT) using the plane wave self-consistent field as implemented in the CASTEP code [11]. The periodic boundary conditions and plane-wave expansion of the wave function were employed. The generalized gradient approximation in the scheme of the Perdew-Burke-Ernzerhof (PBE) [12] function was used to calculate the exchange-correlation potential, and the PAW pseudopotential was applied to describe electron-ion interactions. A vacuum space of ~20Å was included to avoid the spurious interactions between periodic slabs. The electron densities were self-consistently converged to an energy difference of at least 10^{-5} eV. All the atoms were allowed to fully relax until the forces exerted on each atom are less than 0.01 eV/Å during structural optimization. A plane-wave basis set was employed with a kinetic energy cutoff of 400 eV, and the 2D Brillouin zone is sampled using a 4x4x1 mesh-grid. The position coordinates of the atoms in unit cell and lattice parameters are given as input to the software with necessary conditions set by input parameters for cell relaxation. After relaxing the cell for minimum energy configuration, the lattice parameter of the structure is calculated.

In this study, we investigated the opto-electronic and magnetic property changes under an electric field on both SV and Vanadium adatom adsorption BlueP materials. The external electric fields are applied in directions parallel and perpendicular to the material planes. To examine the stability of the atomic defects, we defined the formation energy of a single vacancy as following:

$$\Delta E_f = E_{def} + N\mu_P - E_{pristine} \quad (1)$$

where E_{def} and $E_{pristine}$ are the total energy of the single vacancy and pristine BlueP respectively, N is the number of P atom removal from a pristine BlueP, which is one in the case of a single vacancy BlueP, μ_P is the energy per atom of pristine BlueP.

We also defined the adsorption energy of a Vanadium adatom (V-adatom) on a pristine BlueP as

$$\Delta E_{ads} = E_{BP+V} - E_V - E_{pristine} \quad (2)$$

where E_{BP+V} is the total energy of a V-adatom absorbed on a pristine BlueP, and E_V is the energy per atom of a Vanadium body-centered cubic (bcc) crystal structure.

We followed the standard procedure implemented in the CASTEP code to calculate the real (ε_1) and the imiginary (ε_2) parts of the dielectric constant and then defined the optical absorption coefficient ($\alpha(\omega)$) as the decay constant for the electric field of a plane wave propagating through matter [13]:

$$\alpha(\omega) = \sqrt{2}\omega\sqrt{\varepsilon_1(\omega)^2 + \varepsilon_2(\omega)^2 - \varepsilon_1(\omega)} \quad (3)$$

3. Numerical Results and Discussions

3.1. Stability and Geometrical Configurations

The energetically favorable crystal configurations of pristine and SV BlueP sheets are shown in Figs. 1 (a-b). The primitive unit cell of the optimized BlueP is a hexagonal lattice with a space group of D_{3d}^3, which is in an excellent agreement with previous work [14, 15]. The lattice constant, the P-P bond length, the buckling height (h) between the upper and the lower layer P atoms, and the bond angle (θ) of this primitive cell are 3.32 Å and 2.284 Å, 1.22 Å, $\theta = 93.97^0$, respectively, in quanlitative agreement with ref. [16]. Note that BlueP configurations reported in the literature fall into two prominent space groups of D_{3d}^3 (as presented in this study and in refs. [14]–[19]) and C_{3v} (i.e. ref. [20]). Albeit the electronic property of these optimized BlueP configurations may not alter much, the defect structures created by these configurations may behave significantly different. We obtained the lattice constants of the optimized pristine BlueP of a = 13.2874 Å, b = 13.2874 Å, and c = 20 Å. The morphology of the optimized SV system is in good agreement with Vergara, et al.'s work [21] for an armchair BlueP nanotube. As shown in Table 1, the P-P bond lengths of the SV system are slightly shorter than the corresponding bond lengths of pristine BlueP. The formation energy of the SV system is about 2.48 eV (Table 3, at a zero electric field) in good agreement with Refs. [18, 20, 22].

The second investigated defective BlueP is a pristine BlueP sheet adsorbing a V-adatom. To find the optimal configuration of a V-adatom on a pristine BlueP, we first placed a V-adatom at four possible adsorption sites including a hollow (H) site at the center of a hexagon ring, a bridge (B) site at the P–P bond center, a top (T) site at the upper layer P atoms, and a valley (V) site at the lower layer P atoms (Figure 1a). The initial distance between the V-adatom and the nearest P atom in a BlueP sheet is set to at least 3.0 Å. After optimization, using in eq. 2, we obtained the adsorption energy for H-, T-, V- and B-sites of 1.54 eV, 1.60 eV, 1.70 eV, and 1.70 eV respectively. The positive adsorption energy values indicate that these adsorbing systems are less energetically stable than the pristine BlueP. Among these optimized configurations, the most stable configuration is at a H-site (Figure 1c). Table 2 presents the P-P bonds and V-P bonds around the V-adatom. As recognized simultaneously in Table 2 and Figure 1c, the hexagonal ring around the V-adatom is compressed towards this adsorption atom, and the hexagonal ring is strongly distorted at the 4th and 6th P atoms. After optimization, we observe three additional chemical bonds established from the upper layer P atoms in the nearest hexagonal ring of the V-adatom. Thus, the adsorption of a V-adatom on a pristine BlueP is a chemisorption. From the side view of the V-adatom BlueP sheet (Figure 1c), it is obvious that after the V-adatom is adsorbed, we

observe a concave form with a peak at the V-adatom, predicting a significant electronic as well as photonic property changes in the perpendicular direction to the material plane.

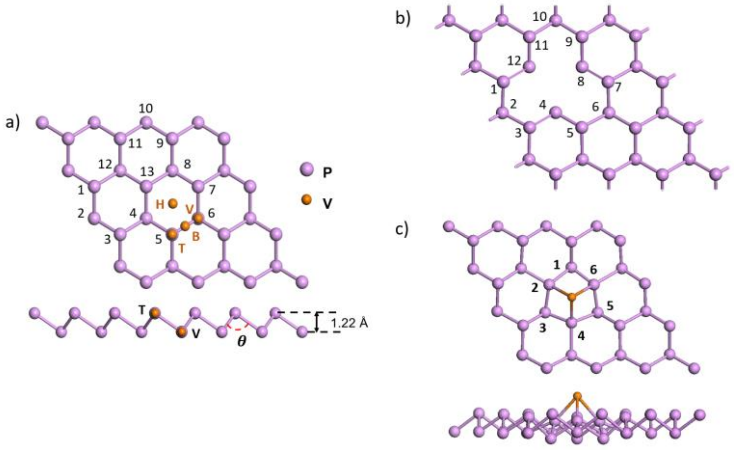

Figure 1. The optimized configurations of pristine (a), single vacancy (SV) (b), and H-site Vanadium adatom (c) BlueP: a) Top-view and side-view of the geometrical stabilized pristine BlueP with thirteen labelled P atoms and four possible adsorption sites including a hollow (H) site at the center of a hexagon ring, a bridge (B) site at the P–P bond center, a top (T) site at the upper layer P atoms, and a valley (V) site at the lower layer P atoms. b) Top-view of the most favorable SV BlueP structure with twelve remaining labelled P atoms. c) Top-view and side-view of the most stable adsorption configuration of H-site V-adatom BlueP with six labelled P atoms. The P and V atoms are shown in blue and orange balls, respectively.

Table 1. Bond lengths of the optimized pristine and single vacancy (SV) BlueP sheets. The labelled P atoms in this Table are presented in Figure 1 (a-b). The bond lengths are in the unit of Angstrom

Bond length (Å)	P1-P12	P3-P4	P4-P5	P7-P8	P8-P9	P11-P12
Pristine	2.27195	2.27136	2.27155	2.27156	2.27177	2.27147
Single vacancy	2.23462	2.23514	2.23505	2.23471	2.23402	2.23394

Table 2. Bond lengths of the optimized H-site Vanadium adatom BlueP. The labelled P atoms in this Table are presented in Figure 1 (c). The bond lengths are in the unit of Angstrom

Bond	P1-P2	P2-P3	P3-P4	P4-P5	P5-P6	P6-P1	V-P2	V-P4	V-P6
Bond length (Å)	2.243	2.241	2.238	2.239	2.241	2.243	2.420	2.404	2.412

3.2. Electronic and Magnetic Properties

We now turn our attention to the electronic band structures of pristine and defect BlueP. Figure 2a shows that pristine BlueP has an indirect bandgap with the valence band maximum (VBM) along the Γ-K region while the conduction band minimum (CBM) along the Γ-M line. The calculated bandgap is about 1.74 eV in qualitative agreement with previous reports [18, 19, 23]. The presence of a SV site induces essential electronic modification to a BlueP thin film: as shown in Figure 2b, both spin-up and spin-down bands cross the Fermi level at the Γ point; thus, this material becomes half-metallic when a P atom is removed. We observe four localized states around the Fermi level (two spin-up and two spin-down states), and the charge densities mainly localize at the 4^{th}, 8^{th} and 12^{th} P atoms. The resulting up- and down-spin states also introduce spin polarizations to the SV system with a magnetic moment of $0.5\mu_B$.

More interestingly, V-adatom BlueP even exhibits a substantial magnetic modification. A V-adatom with an electronic orbital configuration of [Ar] $4s^2$ $3d^3$ induces a phenomenon magnetic moment of 1.37 μ_B (as shown in Table 4 at zero electric field) when being adsorbed on a bare BlueP. This is in line with the prediction reported in Ref. [22] for an adsorption atom with an odd number of electrons. The strong interaction between the TM atom and the pristine BlueP definitely modifies the electronic structure of the defective material: the conduction band states come down to the Fermi level to turn this material to metal, and the magnetic moment and the charge density are mainly localized at the V-adatom. Furthermore, as seen in the DOS figures of the SV and the V-adatom systems (Figure 2b and 2c), while the SV system shows a symmetrical DOS behavior for both up- and down-spin states, the DOS of the V-adatom system is significantly asymmetrical, especially in the energy range from 0 eV to -1.5 eV in the valence band. This observation suggests strong spin hybridization when adsorbing a TM atom on this system.

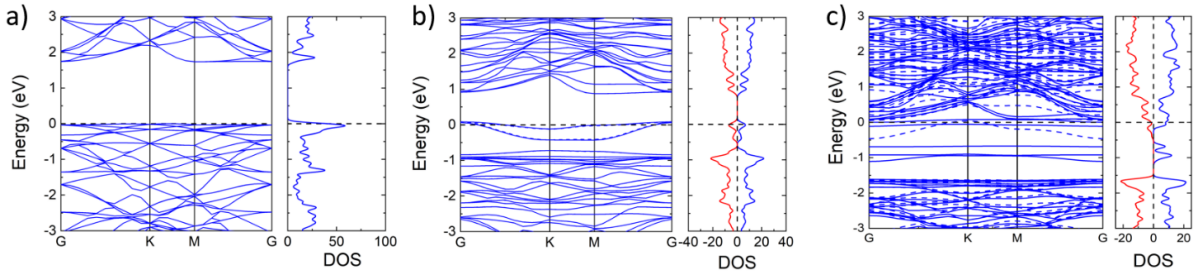

Figure 2. The band structures (BS) and density of states (DOS) of pristine (a), SV (b), and V-adatom BlueP sheets. In the b) and c) BS figures, the blue dashed lines denote spin-down bands, while the solid lines are for the spin-up bands. In the b) and c) DOS of figures, the red lines demonstrate the spin-down DOS and the blue lines present the spin-up DOS. The Fermi level is set to zero and indicated by a black dashed line.

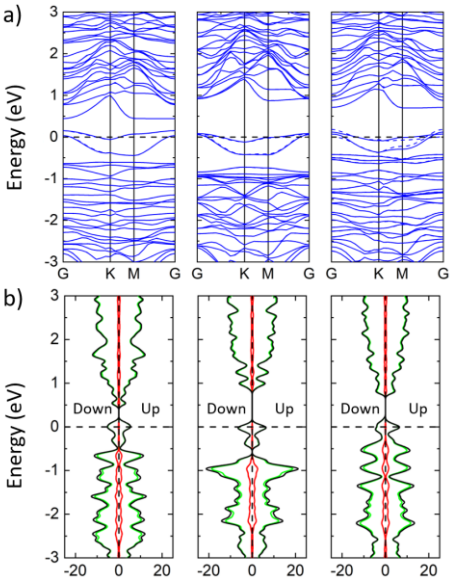

Figure 3. Band structures (a) and density of states (b) of SV BlueP with different external electric fields: from left to right, the applied electric fields are -0.6 eV, zero eV, and +0.6 eV, respectively. The dashed blue lines indicate down-spin while the solid lines are for up-spin states. The Fermi level is set to zero and indicated by a black dashed line.

Table 3. Formation energy (eV) and magnetic moments (μ_B) of SV BlueP as a function of applied electric fields. The electric field is applied in a direction parallel to the material plane.

Electric field (eV)	ΔE_f (eV)	Magnetic moments (μ_B)
-0.6	2.67	0.07
0	2.48	0.50
0.6	-7.95	0.08

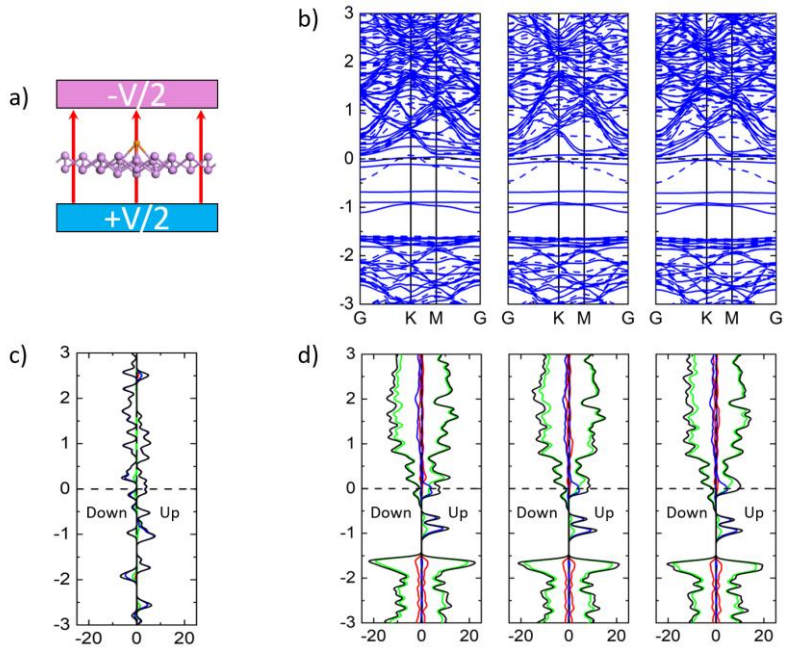

Figure 4. Band structures (BS) and density of states (DOS) of V-adatom BlueP under an external electric field. (a) A sketch of an applied electric field on a V-adatom BlueP. (b) and (d) BS and DOS of this system under an applied electric field: from left to right, the applied electric fields are -0.6 eV, zero eV, and +0.6 eV, respectively. (c) DOS of a V body-centered cubic (bcc) crystal. For BS figures, spin-up states are plotted in the solid lines while spin-down states are in dashed lines. For DOS figures, red, green, and blue curves denote the PDOS projected on the s, p, d orbits. Black curve is the total DOS of the system. The Fermi level is set to zero and indicated by a black dashed line.

Table 4. Adsorption energy (eV), magnetic moment (μ_B), the change of Hirshfeld electron transfer (ΔQ) of a H-site V-adatom BlueP as a function of applied electric fields. The electric field is applied in a direction perpendicular to the material plane

Electric field (eV)	ΔE_{ads} (eV)	Magnetic moments (μ_B)	ΔQ (e)
-0.6	1.30	1.08	-0.11
0	1.54	1.37	0
0.6	0.28	0.95	0.16

We now investigate the effect of an external electric field on the defect engineering BlueP. The electric fields were applied in directions parallel to the SV and perpendicular to the V-adatom planes, respectively. We chose electric field strengths of +0.6 eV and -0.6 eV, which is strong enough to magnetically perturb the systems but weak enough not to destroy the materials. In the case of SV

systems, the electric field actually turns ON/OFF the system magnetic moments: the conduction band of the SV system with a -0.6 eV electric field moves down towards the Fermi level and the valence band of the SV system energized by the opposite electric field clearly moves up to the Fermi line (Figure 3); consequently, the electric field almost switches OFF the magnetic moments in both cases (Table 3). Table 3 also shows that under a positive electric field, the formation energy of this system even switches its sign to a negative value of -7.95 eV, pointing out that the electric field in this direction helps stabilize the SV BlueP sheet. These phase transformations from semiconductors to half-metallic or to metallic materials under an external electric field are in line with the recent observations of black phosphorene nanoribbons [24] and blue phosphorene/stanene heterostructures [25].

Table 5. Magnetic moment (μ_B) of a H-site V-adatom BlueP with an extra electron (-1e: one electron removal and +1e: one electron added) as a function of applied electric fields. The electric field is applied in a direction perpendicular to the material plane

Electric field (eV)	Magnetic moments (μ_B)		
	-1e	0	+1e
-0.6	0.75	1.08	2.51
0	0.41	1.37	0.99
0.6	0.70	0.95	1.55

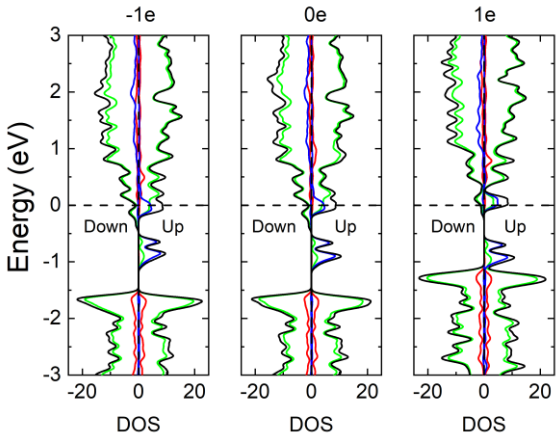

Figure 5. Partial density of states (PDOS) of V-adatom BlueP under a -0.6eV external electric field with different charge filling configurations: from left to right, with an electron removal (-1e), without additional charge, with an electron added (+1e). Red, green, and blue curves denote the PDOS projected on the s, p, d orbits. Black curve is the total DOS of the system. The Fermi level is set to zero and indicated by a black dashed line.

In the case of V-adatom BlueP, the magnetic moments of the energetic systems are slightly reduced under the electric fields in both directions. However, in Table 4, the local magnetization and charge transfers between the V and P atoms show rich behavior: under a positive electric field (the direction towards the V-adatom, Figure 4a), more charge is localized in the V-adatom ($\Delta Q = 0.16e$) and the magnetic moment of this atom is slightly reduced. Contrary to the positive direction of the electric field, more charges are depleted near the region between the V-adatom and the BlueP sheet ($\Delta Q = -0.11e$), the magnetic moment of the V-adatom is slightly weaker compared to the system at a zero electric field. Note that the electron transfer (ΔQ) is defined as the Hirshfeld charge difference between the V- adatom with and without an external electric field as suggested by Yun *et al.* [26]. In Figure 4, the band structures and the density of states of V-adatom BlueP do not show a fundamental difference under external electric

fields. The two flat bands in between -1eV and the Fermi level are mainly contributed by the d-orbital of the V-adatom. At this level, it is difficult to enlighten the origin of the electron transfer and magnetic moment changes of these systems. Following the suggestion of Huang, *et al.* [27] and Srivastava, *et al.* [22] by charging the substrate with an additional electron, we can artificially control the magnetic properties of the systems. Figure 5 and Table 5 clearly indicate that by adding an electron to the systems, the PDOS of the d orbitals and the hybridized p orbitals in the valence bands show a prominent vertical shift towards the Fermi level, resulting in a sudden increase of the magnetic moments under a -0.6eV electric field. Thus, the increase of the magnetic moment is caused by the escape of the charge from the d orbital of the V-adatom, which increases the unbalances between the up- and down-spin states towards the Fermi level. Analogous observation is also reported for Fe-adatom graphene under an external electric field [26].

3.3. Optical Properties

In the previous section, we have shown a novel method to control the charge carrier mobility of defect BlueP. In this section, we further investigate the correlation between the mobile charges and the absorption coefficient spectra of the defect systems. By computing the complex dielectric function $\varepsilon(\omega) = \varepsilon_1(\omega) + i\varepsilon_2(\omega)$ and using the eq. 3, we can calculate the absorption coefficient spectra of our defect BlueP under electric fields. Figures 6 and 7 present the absorption coefficients of the SV and V-adatom BlueP under electric fields in the directions parallel to and perpendicular to the material plane, respectively. In general, the absorption coefficients of SV and V-adatom systems are at least doubled than that of the pristine BlueP, suggesting that the light absorption competency of these defect systems is significantly improved. Furthermore, by increasing the electric field strengths up to 0.6 eV/Å/electron, the absorption coefficients show a strong correlation to electric field perturbation. In the case of SV BlueP, the absorption coefficient is more pronounced in the x-polarization with two dominant peaks at $4.7\text{x}10^4$ cm^{-1} (under a 0.6 eV electric field) and $3.9\text{x}10^4$ cm^{-1} (under a -0.6 eV field) in the ultra-violet region and a peak at $1.1\text{x}10^4$ cm^{-1} (under a -0.6 eV field) from an incident wavelength of 700 nm. For V-adatom BlueP, in the z-polarization, under a -0.6 eV electric field, the optical absorption spectra show an apparent red shift towards the visible light range with a prominent peak of 10^4 cm^{-1}. This absorption enhancement, which is first observed by first-principles method, is crucial to develop the next generation solar cells using BlueP layers.

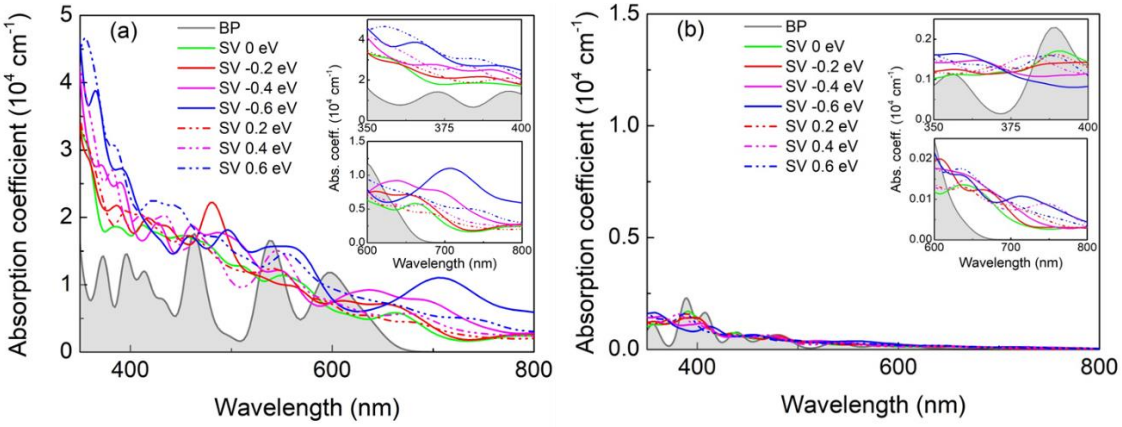

Figure 6. Absorption coefficient of SV BlueP as a function of applied electric fields. The electric field is applied in a direction parallel to the material plane. (a) and (b) are the absorption coefficient spectra in the x- and z-polarizations, respectively. Absorption coefficient spectra of pristine BlueP are also included as a reference.

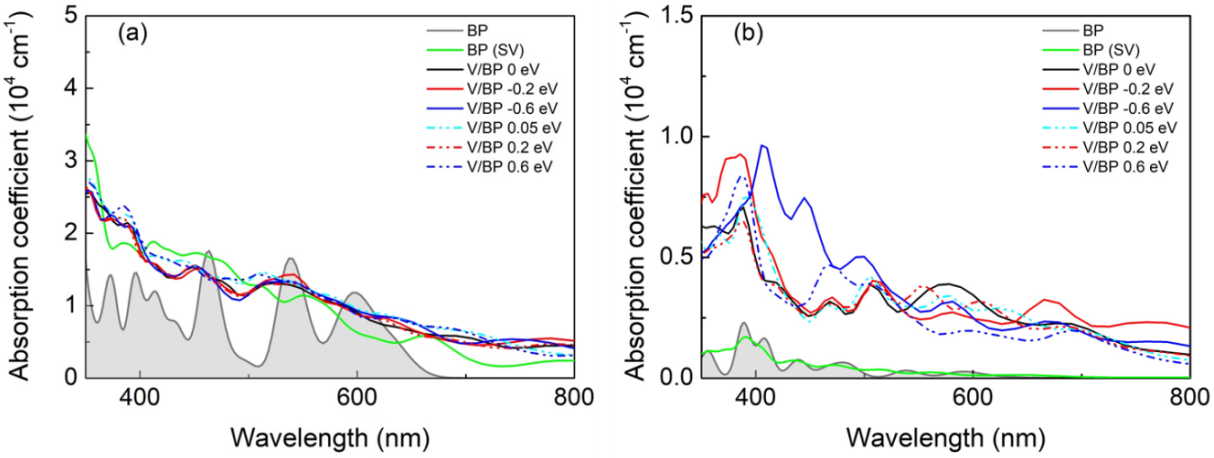

Figure 7. Absorption coefficient of V-adatom BlueP as a function of applied electric fields. The electric field is applied in a direction perpendicular to the material plane. (a) and (b) are the absorption coefficient spectra in the x- and z- polarizations, respectively. Absorption coefficient spectra of pristine and SV BlueP are also included as a reference.

4. Conclusion

In conclusion, using DFT calculations, we have systematically studied the effects of external electric fields on the electronic, magnetic and optical absorption properties of SV and V-adatom BlueP thin films. We show that the optical absorption coefficients of the heterostructures are significantly enhanced compared to that of the bare BlueP. When applying electric fields in directions parallel to the SV and perpendicular to the V-adatom BlueP planes, we observe prominent red shifts of the absorption spectra towards the visible light range. Furthermore, the external electric fields also allow us to switch ON/OFF the magnetic moments the defective systems. By charging the substrate with an additional electron, we show that the magnetic moment changes under the external electric fields is originated from the d and the hybridized p orbitals of the V-adatom. Our results open a novel approach to develop tunable magnetism as well as optical absorption capacity of the next generation solar technology.

Acknowledgments

This research is funded by Vietnam National Foundation for Science and Technology Development (NAFOSTED) under grant number 103.01-2018.308.

References

[1] P. Vogt et al., Silicene: Compelling Experimental Evidence for Graphenelike Two-dimensional Silicon, Physical Review Letters, Vol. 155501, 2012, pp. 1-5, https://doi.org/10.1103/PhysRevLett.108.155501.

[2] B. Feng et al., Experimental Realization of Two-dimensional Boron Sheets, Nature Chemistry, Vol. 8, No. 6, 2016, pp. 563-568, http://dx.doi.org/10.1038/nchem.2491.

[3] H. Liu et al., Phosphorene: An Unexplored 2D Semiconductor with a High Hole Mobility, ACS Nano, Vol. 8, No. 4, 2014, pp. 4033-4041, https://doi.org/10.1021/nn501226z.

[4] L. Li et al., Black Phosphorus Field-effect Transistors, Nature Nanotechnology, Vol. 9, No. 5, 2014, pp. 372-377, https://doi.org/10.1038/nnano.2014.35.

[5] Z. Y. A. Balushi et al., Two-dimensional Gallium Nitride Realized Via Graphene Encapsulation, Nature Materials, Vol. 15, No. 11, 2016, pp. 1166-1171, https://doi.org/10.1038/nmat4742.

[6] Q. H. Wang, K. Kalantar-Zadeh, A. Kis, J. N. Coleman, M. S. Strano, Electronics and Optoelectronics of Two-dimensional Transition Metal Dichalcogenides, Nature Nanotechnology, Vol. 7, No. 11, 2012, pp. 699-712, https://doi.org/10.1038/nnano.2012.193.

[7] J. Qiao, X. Kong, Z. X. Hu, F. Yang, W. Ji, High-mobility Transport Anisotropy and Linear Dichroism in Few-layer black Phosphorus, Nature Communications, Vol. 5, No. 1, 2014, pp. 4475, https://doi.org/10.1038/ncomms5475.

[8] W. Zhang et al., Epitaxial Synthesis of Blue Phosphorene, Small, Vol. 14, No. 51, 2018, pp. 1804066, https://doi.org/10.1002/smll.201804066.

[9] W. Yu, Z. Zhu, C. Y. Niu, C. Li, J. H. Cho, Y. Jia, Dilute Magnetic Semiconductor and Half-Metal Behaviors in 3d Transition-Metal Doped Black and Blue Phosphorenes: A First-Principles Study, Nanoscale Research Letters, Vol. 11, No. 1, 2016, pp. 1-9, https://doi.org/10.1186/s11671-016-1296-x.

[10] T. Hu, J. Hong, First-principles Study of Metal Adatom Adsorption on Black Phosphorene, The Journal of Physical Chemistry C, Vol. 119, No. 15, 2015, pp. 8199-8207, https://doi.org/10.1021/acs.jpcc.5b01300.

[11] S. J. Clark et al., First Principles Methods using CASTEP, Zeitschrift Für Kristallographie - Crystalline Materials, Vol. 220, No. 5-6, 2005, pp. 567-570, https://doi.org/10.1524/zkri.220.5.567.65075.

[12] J. P. Perdew, K. Burke, M. Ernzerhof, Generalized Gradient Approximation Made Simple, Physical Review Letters, Vol. 77, No. 18, 1996, pp. 3865-3868, https://doi.org/10.1103/PhysRevLett.77.3865.

[13] J. Patterson, B. Bailey, Optical Properties of Solids, in Solid-State Physics: Introduction to the Theory, Berlin, Heidelberg: Springer Berlin Heidelberg, 2010, pp. 545-590.

[14] Y. Aierken, D. Cakir, C. Sevik, F. M. Peeters, Thermal Properties of Black and Blue Phosphorenes from a First-principles Quasiharmonic Approach, Physical Review B, Vol. 92, No. 8, 2015, pp. 81408, https://doi.org/10.1103/PhysRevB.92.081408.

[15] J. Xie, M. S. Si, D. Z. Yang, Z. Y. Zhang, D. S. Xue, A Theoretical Study of Blue Phosphorene Nanoribbons Based on First-principles Calculations, Journal of Applied Physics, Vol. 116, No. 7, 2014, pp. 73704, https://doi.org/10.1063/1.4893589.

[16] G. Yang, Z. Xu, Z. Liu, S. Jin, H. Zhang, Z. Ding, Strain - and Fluorination-Induced Quantum Spin Hall Insulators in Blue Phosphorene: A First-Principles Study, The Journal of Physical Chemistry C, Vol. 121, No. 23, 2017, pp. 12945-12952, https://doi.org/10.1021/acs.jpcc.7b03808.

[17] Z. Deng, Z. Li, W. Wang, J. She, Vibrational Properties and Raman Spectra of Pristine and Fluorinated Blue Phosphorene, Physical Chemistry Chemical Physics, Vol. 21, No. 3, 2019, pp. 1059-1066, https://doi.org/10.1039/C8CP05699D.

[18] C. Wang, Y. You, J. H. Choi, First-principles Study of Defects in Blue Phosphorene, Materials Research Express, Vol. 7, No. 1, 2020, https://doi.org/10.1088/2053-1591/ab59fc.

[19] K. D. Pham et al., Two-dimensional Blue Phosphorene–BAs vdW Heterostructure With Optical And Photocatalytic Properties: a First-principles Study, RSC Advances, Vol. 11, No. 21, 2021, pp. 13025-13029, https://doi.org/10.1039/D1RA00004G.

[20] M. Sun, J. P. Chou, A. Hu, U. Schwingenschlögl, Point Defects in Blue Phosphorene, Chemistry of Materials, Vol. 31, No. 19, 2019, pp. 8129-8135, https://doi.org/10.1021/acs.chemmater.9b02871.

[21] J. M. Vergara, E. Flórez, M. E. Mora-Ramos, J. D. Correa, Effects of Single Vacancy On Electronic Properties of blue-phosphorene nanotubes, Materials Research Express, Vol. 7, No. 1, 2020, pp. 15042, https://doi.org/10.1088/2053-1591/ab66a6.

[22] P. Srivastava, K. P. S. S. Hembram, H. Mizuseki, K. R. Lee, S. S. Han, S. Kim, Tuning the Electronic and Magnetic Properties of Phosphorene by Vacancies and Adatoms, The Journal of Physical Chemistry C, Vol. 119, No. 12, 2015, pp. 6530-6538, https://doi.org/10.1021/jp5110938.

[23] Z. Zhu, D. Tománek, Semiconducting Layered Blue Phosphorus: A Computational Study, Physical Review Letters, Vol. 112, No. 17, 2014, pp. 1-5, https://doi.org/10.1103/PhysRevLett.112.176802.

[24] M. U. Farooq, A. Hashmi, J. Hong, Ferromagnetism controlled by electric field in tilted phosphorene nanoribbon, Scientific Reports, Vol. 6, No. 1, 2016, p. 26300, https://doi.org/10.1038/srep26300.

[25] J. Chen, K. Ma, J. Xiao, L. Xu, X. Dai, Z. Wang, Modulation of the Electronic Properties of Blue Phosphorene/Stanene Heterostructures By Electric Field And Interlayer Distance, Results in Physics, Vol. 34, 2022, pp. 105252, https://doi.org/10.1016/j.rinp.2022.105252.

[26] K. H. Yun, M. Lee, Y. C. Chung, Electric Field as a Novel Switch for Magnetization of Fe/Graphene System, Journal of Magnetism and Magnetic Materials, Vol. 362, 2014, pp. 93–96, https://doi.org/10.1016/j.jmmm.2014.03.045.

[27] B. Huang, H. Xiang, J. Yu, S. H. Wei, Effective Control of the Charge and Magnetic States of Transition-Metal Atoms on Single-Layer Boron Nitride, Physical Review Letters, Vol. 108, No. 20, 2012, pp. 206802, https://doi.org/10.1103/PhysRevLett.108.206802.